



Cite this: *RSC Adv.*, 2024, 14, 24970

# Catalytic hydrolysis of methyl mercaptan and methyl thioether on hydroxyl-modified ZrO<sub>2</sub>: a density functional theory study†

Guihua Zhang<sup>a</sup> and Xin Song  <sup>\*bc</sup>

The purification and removal of organic sulfur from natural gas is conducive to increasing the added value of natural gas and reducing environmental pollution. In this study, the adsorption properties of methyl mercaptan (CH<sub>3</sub>SH), dimethyl sulfide (C<sub>2</sub>H<sub>6</sub>S) and H<sub>2</sub>O on the surface of hydroxyl-modified ZrO<sub>2</sub> were investigated using density functional theory (DFT) calculations. Additionally, a reaction mechanism was proposed for hydroxyl-modified ZrO<sub>2</sub> catalyzing the hydrolysis of CH<sub>3</sub>SH and C<sub>2</sub>H<sub>6</sub>S. The chemisorption of H<sub>2</sub>O molecules on the catalyst surface is attributed to H–O and H–Zr bonds. The chemisorption of CH<sub>3</sub>SH and C<sub>2</sub>H<sub>6</sub>S on the catalyst surface is attributed to Zr–S bonds. Competitive adsorption between the three gases exists only between CH<sub>3</sub>SH and C<sub>2</sub>H<sub>6</sub>S. It reveals the water-resistant properties of hydroxyl-modified ZrO<sub>2</sub> in desulfurization. The adsorption energies of the three gas molecules on the hydroxyl-modified ZrO<sub>2</sub> surface are in the order of CH<sub>3</sub>SH – (Zr) > C<sub>2</sub>H<sub>6</sub>S – (Zr) > H<sub>2</sub>O – (OH). The natural hydrolysis of CH<sub>3</sub>SH and C<sub>2</sub>H<sub>6</sub>S is a heat-absorbing process that cannot occur spontaneously. The rate-determining step for CH<sub>3</sub>SH catalytic hydrolysis is the formation of CH<sub>3</sub>O. The fracture of CH<sub>3</sub>SHO is the rate-determining step for C<sub>2</sub>H<sub>6</sub>S catalytic hydrolysis. The depletion of the surface hydroxyl groups can be replenished by the dissociation of H<sub>2</sub>O molecules. Hydroxyl-modified ZrO<sub>2</sub> facilitated the hydrolysis process of CH<sub>3</sub>SH to a greater extent than that of C<sub>2</sub>H<sub>6</sub>S. This study provides theoretical guidance for industrial applications and the design of hydroxyl-containing hydrolysis catalysts.

Received 23rd May 2024  
Accepted 29th July 2024

DOI: 10.1039/d4ra03801k

rsc.li/rsc-advances

## 1. Introduction

In light of the imperative to sustainably develop the global climate and environment, the energy structure is undergoing continual optimization, with natural gas assuming an increasingly pivotal role in the global primary energy mix. Sulfides such as hydrogen sulfide (H<sub>2</sub>S), carbonyl sulfide (COS), methyl mercaptan (CH<sub>3</sub>SH) and dimethyl sulfide (C<sub>2</sub>H<sub>6</sub>S) are common harmful impurities in natural gas, which not only reduce the value of natural gas utilization but also cause corrosion of equipment and environmental pollution.<sup>1,2</sup> Therefore, the purification of sulfur-containing impurities in natural gas is conducive to environmental protection and effective utilization of natural gas. The purification technologies for H<sub>2</sub>S and COS are relatively mature, so the key to natural gas desulfurization is the purification of CH<sub>3</sub>SH and C<sub>2</sub>H<sub>6</sub>S.<sup>3</sup>

The removal of CH<sub>3</sub>SH and C<sub>2</sub>H<sub>6</sub>S from natural gas is more effectively and stably accomplished using dry methods such as adsorption, catalytic oxidation, catalytic decomposition, and catalytic hydrolysis.<sup>4–7</sup> Among these methods, the catalytic hydrolysis method has been receiving increasing attention due to its low secondary pollution and high value of by-products. Zhang *et al.* investigated the role of H<sub>2</sub>O molecules on CH<sub>3</sub>SH removal over Cu/C-PAN catalyst.<sup>6</sup> It was demonstrated that water promotes the adsorption of CH<sub>3</sub>SH at low temperatures and its hydrolysis at high temperatures. While H<sub>2</sub>S is the primary hydrolysis product, the reaction temperature and active components influence the type and quantity of the final product. This can diminish the desulfurization stability of the catalyst. Metal oxides, such as ZrO<sub>2</sub>, are frequently employed in the purification of gaseous pollutants, exhibiting high reaction stability and resistance to sulfur poisoning.<sup>8–10</sup> This property is conducive to the stability of the catalytic hydrolysis process of organic sulfur and the prolongation of catalyst service life.<sup>11</sup> Therefore, ZrO<sub>2</sub> can be considered a potential hydrolysis catalyst for the purification of organic sulfur. Furthermore, hydroxyl groups play a pivotal role in the hydrolysis of organic sulfur. These groups are primarily derived from the dissociation of H<sub>2</sub>O molecules and the metal-hydroxyl functional groups on the surface.<sup>12</sup> Song *et al.* investigated the mechanism of the COS hydrolysis reaction over a MgAlCeO<sub>x</sub> hydrothermalite-like catalyst.<sup>13</sup>

<sup>a</sup>Department of Mechanical Engineering, Wuhan Vocational College of Software and Engineering, Wuhan 430205, China

<sup>b</sup>Faculty of Environmental Science and Engineering, Kunming University of Science and Technology, Kunming 650500, China. E-mail: save24176@126.com; Fax: +86-0871-65926040; Tel: +86-0871-65926040

<sup>c</sup>Pingxiang Huaxing Environmental Protection Engineering Technology Co., Ltd, Pingxiang, 337022, China

† Electronic supplementary information (ESI) available. See DOI: <https://doi.org/10.1039/d4ra03801k>


The presence of hydroxyl M–OH on the catalyst surface enhanced the hydrolysis process while providing more sites for organic sulfur adsorption. Therefore, hydroxylation modification on the  $\text{ZrO}_2$  surface can be employed to enhance the hydrolysis process of organic sulfur. However, studies on the catalytic hydrolysis of  $\text{CH}_3\text{SH}$  and  $\text{C}_2\text{H}_6\text{S}$  using hydroxylated  $\text{ZrO}_2$  are lacking, and the reaction mechanism has not been clarified. Therefore, it is necessary to propose a catalytic hydrolysis reaction mechanism of  $\text{CH}_3\text{SH}$  and  $\text{C}_2\text{H}_6\text{S}$  on hydroxyl  $\text{ZrO}_2$  through theoretical studies.

This work presents a systematic investigation of the competitive adsorption process of  $\text{CH}_3\text{SH}$  and  $\text{C}_2\text{H}_6\text{S}$ , the catalytic hydrolysis reaction mechanism, and the catalytic role of surface hydroxyls. The investigation is conducted using a density-functional theory (DFT) approach. Additionally, the effects of  $\text{ZrO}_2$  and surface hydroxyl groups on the hydrolysis reaction pathway are presented.

## 2. Computational method

$\text{ZrO}_2$  has been identified as a suitable catalyst for hydrolysis reactions in experimental and theoretical studies.<sup>14</sup> Additionally, the  $\text{ZrO}_2(100)$  surface exhibits suitability for surface hydroxylation modification.<sup>15</sup> Therefore, in this study, cubic  $\text{ZrO}_2$  was employed to construct hydroxyl-modified  $\text{ZrO}_2$ . The geometries and energies for the catalyst (hydroxyl-modified  $\text{ZrO}_2$ ), reactants ( $\text{CH}_3\text{SH}$ ,  $\text{C}_2\text{H}_6\text{S}$ ,  $\text{H}_2\text{O}$ ), intermediates (IM), products, and transition states (TS) were calculated using Material Studio 2017 with the Dmol<sup>3</sup> module.<sup>16,17</sup> The GGA/PBE method employed herein provides a precise description of the interactions between electrons and encompasses a diverse range of material systems, thereby making it a highly prevalent choice in studies involving metal-containing catalytic systems.<sup>18</sup> The calculation work employed the GGA/PBE method with a DNP 4.4 basis and spin-polarized set.<sup>19</sup> The spin was set to unrestricted and the total charge was set to 0. In order to calibrate the energy, the basis set superposition error (BSSE) was taken into account in the calculation. To accurately describe weak interactions, dispersion-corrected density functional theory (DFT-D3 correction) was introduced.<sup>20,21</sup> The SCF, energy, gradient, and displacement convergence tolerances were set to  $1.0 \times 10^{-6}$  Hartree (Ha),  $1.0 \times 10^{-5}$  Ha,  $2.0 \times 10^{-3}$  Ha  $\text{\AA}^{-1}$  and  $5.0 \times 10^{-3}$   $\text{\AA}$ , respectively. The cubic  $\text{ZrO}_2$  was established according to the Crystallography Open Database. The space group of cubic  $\text{ZrO}_2$  was FM-3M, and the lattice parameters are  $a = b = c = 5.070$   $\text{\AA}$ . In this study, a five-layer  $\text{ZrO}_2$  (100) surface with a  $p(3 \times 3)$  supercell size was used. In order to construct the surface hydroxyl group, the  $\text{ZrO}_2(100)$  surface layer is composed of Zr atoms. The vacuum layer is 15  $\text{\AA}$  thick and all atoms are in a relaxed state. Additionally, hydroxyl groups were introduced and immobilised on the surface of Zr atoms to simulate hydroxylated  $\text{ZrO}_2$  surfaces. Therefore, a surface hydroxyl structure of  $\text{Zr-OH}$  is constructed. The aforementioned parameters guarantee the accuracy of the resulting calculations.<sup>18</sup> The transition states were searched, optimised and confirmed using the linear synchronous transit/quadratic synchronous transit/conjugate gradient (LST/QST/CG)

calculation method.<sup>22</sup> The adsorption energies of the binary and ternary systems were calculated using eqn (1) and (2), respectively.  $E_A$ ,  $E_B$  and  $E_C$  represented the energy of the catalysts and the gas molecules.  $E_{\text{BSSE}}$  represented the energy of the basis set superposition error.

$$E_{\text{ads}} = E_{\text{AB}} - E_A - E_B + E_{\text{BSSE}} \quad (1)$$

$$E_{\text{ads}} = E_{\text{ABC}} - E_A - E_B - E_C + E_{\text{BSSE}} \quad (2)$$

## 3. Results and discussion

### 3.1 Adsorption of $\text{CH}_3\text{SH}$ , $\text{C}_2\text{H}_6\text{S}$ and $\text{H}_2\text{O}$ over hydroxyl-modified $\text{ZrO}_2$

The adsorption properties of single and multimolecular gases on hydroxylated modified  $\text{ZrO}_2$  surfaces were investigated. To elucidate the influence of hydroxyl groups on the adsorption process, two distinct adsorption sites were selected for the study: the Zr top site distant from  $\text{Zr-OH}$  (denoted as  $-(\text{Zr})$ ) and the hydroxyl site proximal to  $\text{Zr-OH}$  (denoted as  $-(\text{OH})$ ). The optimized adsorption configurations are depicted in Fig. 1, while the corresponding adsorption energies are presented in Table 1. The adsorption energies of the two gas molecules when simultaneously adsorbed at different sites were examined, and the corresponding adsorption configurations and adsorption energies are shown in Fig. S1 and Table S1,<sup>†</sup> respectively. Following structural optimization based on the calculated adsorption energies, it was determined that adsorption configurations (i), (iv), and (vii) represent the most stable configurations for different bimolecular systems. The current adsorption site was also identified as the global minimum energy point by the sorption module. Consequently, these three conformations were employed in Fig. 1 for comparison with the unimolecular adsorption conformations.

The adsorption energy results indicated that the adsorption of  $\text{H}_2\text{O}$ ,  $\text{CH}_3\text{SH}$ , and  $\text{C}_2\text{H}_6\text{S}$  on the top site of Zr and the hydroxyl site was generated by chemisorption. The  $\text{H}_2\text{O}$  molecules exhibited a tendency to adsorb in close proximity to the  $\text{Zr-OH}$ ,

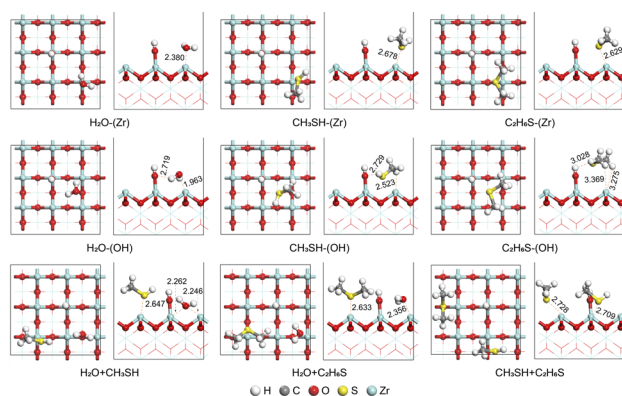


Fig. 1 Optimised adsorption configuration for  $\text{CH}_3\text{SH}$ ,  $\text{C}_2\text{H}_6\text{S}$  and  $\text{H}_2\text{O}$  over hydroxyl-modified  $\text{ZrO}_2$  (bond length in  $\text{\AA}$ ).



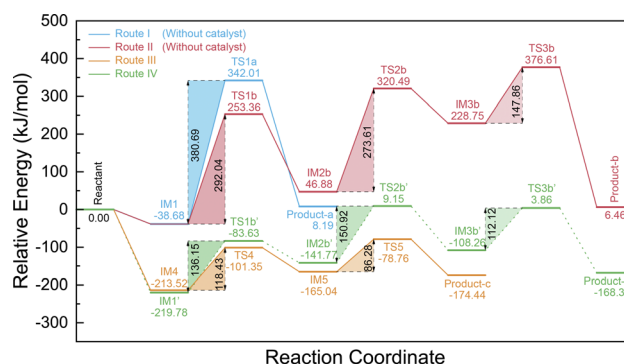
**Table 1** Adsorption energy of CH<sub>3</sub>SH, C<sub>2</sub>H<sub>6</sub>S and H<sub>2</sub>O over hydroxyl-modified ZrO<sub>2</sub>

Adsorptive geometries	Adsorption energy (kJ mol <sup>-1</sup> )
H <sub>2</sub> O – (Zr)	–88.11
H <sub>2</sub> O – (OH)	–123.51
CH <sub>3</sub> SH – (Zr)	–192.68
CH <sub>3</sub> SH – (OH)	–165.83
C <sub>2</sub> H <sub>6</sub> S – (Zr)	–164.89
C <sub>2</sub> H <sub>6</sub> S – (OH)	–114.63
H <sub>2</sub> O + CH <sub>3</sub> SH	–219.78
H <sub>2</sub> O + C <sub>2</sub> H <sub>6</sub> S	–173.37
CH <sub>3</sub> SH + C <sub>2</sub> H <sub>6</sub> S	–148.04

resulting in the formation of H–O and H–Zr bond interactions. The CH<sub>3</sub>SH and C<sub>2</sub>H<sub>6</sub>S molecules exhibited a tendency to adsorb in close proximity to the Zr top site, resulting in the Zr–S bond interactions. This suggests that there is no competitive adsorption relationship between H<sub>2</sub>O and CH<sub>3</sub>SH/C<sub>2</sub>H<sub>6</sub>S, but that there is competitive adsorption between CH<sub>3</sub>SH and C<sub>2</sub>H<sub>6</sub>S. The adsorption energies of the three gas molecules on the hydroxyl-modified ZrO<sub>2</sub> surface are in the order of CH<sub>3</sub>SH–(Zr) > C<sub>2</sub>H<sub>6</sub>S–(Zr) > H<sub>2</sub>O–(OH). This indicates that CH<sub>3</sub>SH can preferentially adsorb on the Zr top site. When CH<sub>3</sub>SH, C<sub>2</sub>H<sub>6</sub>S and H<sub>2</sub>O are adsorbed simultaneously on the hydroxyl-modified ZrO<sub>2</sub> surface, the adsorption energies are in the order of H<sub>2</sub>O + CH<sub>3</sub>SH > H<sub>2</sub>O + C<sub>2</sub>H<sub>6</sub>S > CH<sub>3</sub>SH + C<sub>2</sub>H<sub>6</sub>S. This indicated that H<sub>2</sub>O molecules are more capable of forming a two-gas molecularly stabilized adsorption structure with organosulfur molecules. The adsorption effects were attributed to the interaction between Zr and S/O atoms. Moreover, the adsorption energies of H<sub>2</sub>O and CH<sub>3</sub>SH/C<sub>2</sub>H<sub>6</sub>S are both greater than that of a single gas molecule when they are co-adsorbed on the hydroxyl-modified ZrO<sub>2</sub> surface. The results indicated that the presence of the H<sub>2</sub>O molecule enhances and promotes the adsorption of CH<sub>3</sub>SH/C<sub>2</sub>H<sub>6</sub>S. Conversely, the adsorption energies are lower than those of a single gas when co-adsorption of CH<sub>3</sub>SH and C<sub>2</sub>H<sub>6</sub>S occurs. This is due to the fact that the adsorption of both CH<sub>3</sub>SH and C<sub>2</sub>H<sub>6</sub>S on the ZrO<sub>2</sub> surface is caused by Zr–S interactions, resulting in competitive adsorption at the Zr top site. This results in a reduction in the stability of the adsorption process upon co-adsorption. This further substantiates the competitive adsorption relationship previously discussed. Consequently, the co-adsorption of H<sub>2</sub>O and CH<sub>3</sub>SH was observed to occur most stably on the catalyst surface.

### 3.2 Catalysis hydrolysis routes of CH<sub>3</sub>SH over hydroxyl-modified ZrO<sub>2</sub>

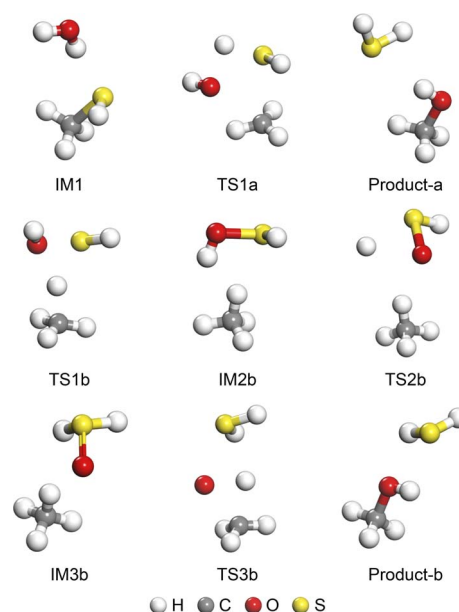
In order to investigate the catalytic hydrolysis of CH<sub>3</sub>SH by hydroxyl groups and ZrO<sub>2</sub>, the natural and catalytic hydrolysis routes of CH<sub>3</sub>SH were investigated. The specific reaction routes are shown in Fig. 2. Route I and Route II are natural hydrolysis reaction processes. Route III is a hydrolysis reaction process involving hydroxyl groups, and Route IV is a hydrolysis reaction process involving only ZrO<sub>2</sub>. The atomic migration process in Route IV was maintained consistent with Route II, which was

**Fig. 2** Reaction routes and reaction energies for CH<sub>3</sub>SH hydrolysis.

employed to assess the catalytic impact of ZrO<sub>2</sub>. During natural hydrolysis, the intermediate (IM) and transition state (TS) structures in Route I and Route II were optimized and presented in Fig. 3. During catalytic hydrolysis, the optimized intermediates and transition states of Route III are shown in Fig. 4.

In Route I, CH<sub>3</sub>SH and H<sub>2</sub>O first undergo physical adsorption to form IM1, releasing 38.68 kJ mol<sup>-1</sup> of energy. After the breaking of the C–S bond in CH<sub>3</sub>SH and the O–H bond in H<sub>2</sub>O, TS1a is formed. This process requires overcoming a significant reaction energy barrier (380.69 kJ mol<sup>-1</sup>). The combination of the hydroxyl group and CH<sub>3</sub> in TS1a, and the combination of the H atom and HS, results in the generation of Product-a (CH<sub>3</sub>OH and H<sub>2</sub>S). The relative energy of Product-a is 8.19 kJ mol<sup>-1</sup>, which suggests that Route I is a heat-absorbing process. Therefore, Route I cannot occur spontaneously.

In Route II, C–S and O–H bonds are initially broken, with H atoms from the dissociation of the H<sub>2</sub>O molecule migrating to CH<sub>3</sub> and the hydroxyl group migrating to HS, forming TS1b. This step requires the consumption of 292.04 kJ mol<sup>-1</sup> of energy

**Fig. 3** IM and TS for CH<sub>3</sub>SH hydrolysis (Route I and Route II).



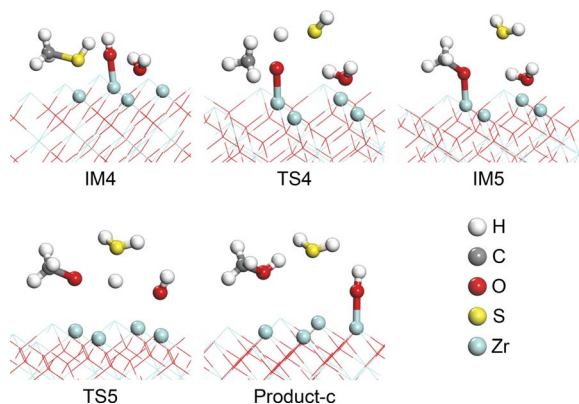


Fig. 4 IM and TS for  $\text{CH}_3\text{SH}$  hydrolysis over hydroxyl-modified  $\text{ZrO}_2$  (Route III).

to be realised. With the combination of C–H and O–S bonds, IM2b was generated. Subsequently, the H atom on the O–H bond in IM2b undergoes an H-transfer. This results in the detachment of the H atom from the O atom and its migration to the S atom, forming  $\text{H}_2\text{SO}$  and generation of IM3b. This process necessitates the overcoming of a reaction energy barrier of  $273.61 \text{ kJ mol}^{-1}$  (from TS2b). Subsequently, the S=O bond in HSHO is broken, and the O atom migrates to the vicinity of  $\text{CH}_4$ , resulting in the breakage of the C–H bond and the production of TS3b. Furthermore, the O atom combines with the H atom and  $\text{CH}_3$  to form  $\text{CH}_3\text{OH}$ . The process of IM3b to Product-b requires the consumption of  $147.86 \text{ kJ mol}^{-1}$  of energy. The reaction energy barriers of the steps in Route II indicate that the reaction rate of Route II is affected by TS1b. Therefore, the production of HSOH is the rate-determining step of Route II. Compared to Route I, Route II has a lower maximum reaction energy barrier, which suggests that Route II is more likely to occur.

In Route III,  $\text{CH}_3\text{SH}$  and  $\text{H}_2\text{O}$  first adsorb around the hydroxyl group to form the stable adsorption structure IM4, which is realized by chemisorption. Next, the C–S bond in  $\text{CH}_3\text{SH}$  and the O–H bond in  $\text{Zr-OH}$  are broken to form TS4, which consumes  $118.43 \text{ kJ mol}^{-1}$  energy. With the formation of S–H and C–O bonds, IM5 is produced. In this step, the  $\text{H}_2\text{O}$  molecule remains intact, and only  $\text{CH}_3\text{SH}$  is converted to  $\text{H}_2\text{S}$  through the surface hydroxyl groups. Then, the  $\text{H}_2\text{O}$  molecule is dissociated into H atoms and hydroxyl groups, while the Zr–O bond is broken. Product-c ( $\text{CH}_3\text{OH}$  and  $\text{H}_2\text{S}$ ) is generated as the hydroxyl group binds to the Zr atom and the H atom migrates to  $\text{CH}_3\text{O}$ . This step necessitates overcoming the  $86.28 \text{ kJ mol}^{-1}$  reaction energy barrier for the generation of TS5. The maximum reaction energy barrier in Route III is the process of TS4 production, which suggests that  $\text{CH}_3\text{O}$  formation is the rate-determining step. In comparison to Route II, the hydroxyl group significantly reduces the maximum reaction energy barrier during hydrolysis. Furthermore, the hydroxyl groups on the surface are capable of facilitating H-transfer, which is essential for the generation of  $\text{H}_2\text{S}$ , as well as the provision of free O atoms for the formation of C–O bonds. The depletion of surface hydroxyl groups can be replenished by the dissociation

of  $\text{H}_2\text{O}$  molecules, which effectively enhances the role of  $\text{H}_2\text{O}$  molecules in the hydrolysis reaction.

The reaction processes of Route IV and Route II are analogous. The change in reaction energy barriers indicates that  $\text{ZrO}_2$  facilitates the hydrolysis process. In contrast to Route II, the participation of  $\text{ZrO}_2$  in the hydrolysis reaction significantly reduces the reaction energy barrier of the HSOH generation step, resulting in the rate-determining step changing to HSHO generation. A comparison of Route III and Route IV revealed that  $\text{ZrO}_2$  and hydroxyl exhibited disparate catalytic effects. The introduction of hydroxyl was found to be capable of further reducing the maximum reaction energy barrier.

### 3.3 Catalysis hydrolysis routes of $\text{C}_2\text{H}_6\text{S}$ over hydroxyl-modified $\text{ZrO}_2$

The natural and catalytic hydrolysis routes of  $\text{C}_2\text{H}_6\text{S}$  were investigated to ascertain the catalytic effect of hydroxyl groups and  $\text{ZrO}_2$ . The four reaction routes are depicted in Fig. 5. Route V and Route VI represent natural hydrolysis reaction processes. Route VII is a hydrolysis reaction process involving hydroxyl groups, and Route VIII is a hydrolysis reaction process involving only  $\text{ZrO}_2$ . The atomic migration process in Route VIII was maintained consistent with that in Route VI, which was employed to assess the catalytic impact of  $\text{ZrO}_2$ . The optimized intermediate (IM) and transition state (TS) structures in Route V and Route VI are illustrated in Fig. 6, and the optimized intermediates and transition states of Route VII are depicted in Fig. 7.

In Route V,  $\text{C}_2\text{H}_6\text{S}$  and  $\text{H}_2\text{O}$  first undergo physical adsorption to form IM6, releasing  $25.46 \text{ kJ mol}^{-1}$  of energy. This adsorption is weaker than that between  $\text{H}_2\text{O}$  and  $\text{CH}_3\text{SH}$ . After the breaking of the C–S bond in  $\text{C}_2\text{H}_6\text{S}$  and the O–H bond in  $\text{H}_2\text{O}$ , TS6a is formed. This process necessitates the overcoming of a reaction energy barrier of  $66.77 \text{ kJ mol}^{-1}$ . The combination of the hydroxyl group and  $\text{CH}_3$  in TS6a, along with the combination of the H atom and  $\text{CH}_3\text{S}$ , results in the generation of Product-a ( $\text{CH}_3\text{OH}$  and  $\text{CH}_3\text{SH}$ ). The relative energy of Product-a is  $26.68 \text{ kJ mol}^{-1}$ , which indicates that Route V is a heat-absorbing process. Consequently, it can be concluded that Route V is not a spontaneous process. Subsequent to this,  $\text{CH}_3\text{SH}$  can undergo further hydrolysis reactions *via* Route II.

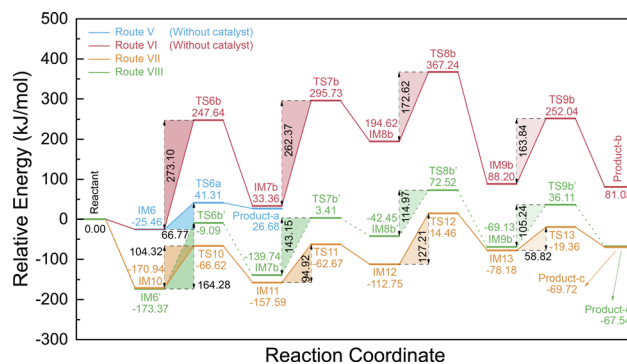


Fig. 5 Reaction routes and reaction energies for  $\text{C}_2\text{H}_6\text{S}$  hydrolysis.



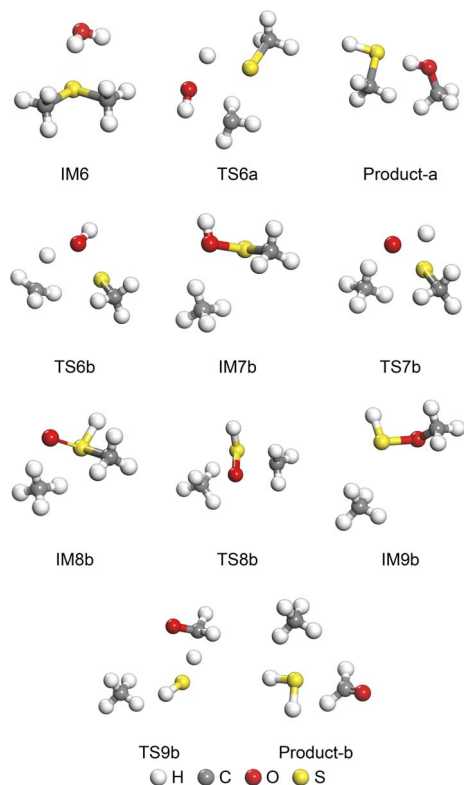


Fig. 6 IM and TS for  $C_2H_6S$  hydrolysis (Route V and Route VI).

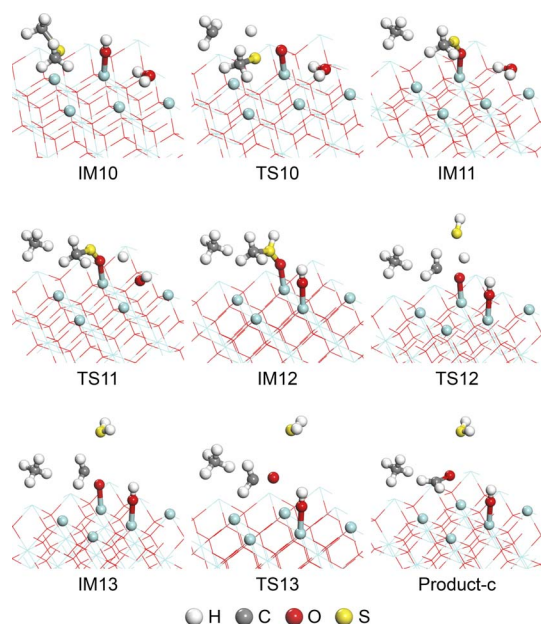


Fig. 7 IM and TS for  $C_2H_6S$  hydrolysis over hydroxyl-modified  $ZrO_2$  (Route VII).

In Route VI, the C–S and O–H bonds are initially broken, with the H atoms from the dissociation of the  $H_2O$  molecule migrating to  $CH_3$  and the hydroxyl group migrating to  $CH_3S$ , forming TS6b. This step requires the consumption of

$273.10 \text{ kJ mol}^{-1}$  of energy to be realised. The combination of the C–H and O–S bonds resulted in the generation of IM7b ( $CH_4$  and  $CH_3SOH$ ). Subsequently,  $CH_3SOH$  in IM7b underwent a H-transfer. The H atom on the O–H bond detached from the O atom and migrated to the S atom to form  $CH_3SHO$ , leading to the generation of IM8b. This process necessitates the overcoming of a reaction energy barrier of  $262.37 \text{ kJ mol}^{-1}$  (from TS7b). Consequently, the C–S bond in  $CH_3SHO$  is broken, and the C–O bond is generated, thus forming  $CH_3OSH$ . The process of IM8b to IM9b requires the consumption of  $172.62 \text{ kJ mol}^{-1}$  of energy. Subsequently, TS9b is generated as the C–H and S–O bonds in  $CH_3OSH$  are broken. The hydrolysis reaction is completed when the H atom completes its migration from the C–H bond to the S–H bond, and the final hydrolysis products are  $CH_4$ ,  $H_2S$ , and  $HCHO$ . The reaction energy barriers of the steps in Route VI indicate that the reaction rate of Route VI is affected by TS6b. Therefore, the production of  $CH_3SOH$  is the rate-determining step of Route VI. Compared to Route V + II, Route VI has a lower maximum reaction energy barrier, which suggests that Route VI is more likely to occur.

In Route VII,  $C_2H_6S$  and  $H_2O$  initially adsorb around the hydroxyl group to form the stable adsorption structure IM10, which is achieved through chemisorption. Subsequently, the C–S bond in  $C_2H_6S$  and the O–H bond in  $Zr-OH$  are broken to form TS10, resulting in the consumption of  $104.32 \text{ kJ mol}^{-1}$  energy. The formation of the C–H and S–O bonds results in the production of IM11. In this step, the  $H_2O$  molecule remains intact, with only  $C_2H_6S$  undergoing conversion to  $CH_3SO$  through the surface hydroxyl groups. Subsequently, the  $H_2O$  molecule is dissociated into H atoms and hydroxyl groups, while S–H is formed. The generation of IM12 occurs through TS11, with a reaction energy barrier of  $94.92 \text{ kJ mol}^{-1}$ . The breaking of C–S and C–H bonds in  $CH_3SO$ , which is accompanied by the migration of H atoms, results in the generation of IM13. This process requires overcoming a  $127.21 \text{ kJ mol}^{-1}$  reaction energy barrier. The hydrolysis reaction is completed when the O atom completes its migration from the  $Zr-O$  bond to the  $C=O$  bond, and the final hydrolysis products are  $CH_4$ ,  $H_2S$ , and  $HCHO$ . The maximum reaction energy barrier in Route VII is the process of TS12 production, which suggests that the fracture of  $CH_3SHO$  is the rate-determining step. Compared to Route VI, the hydroxyl group greatly reduces the maximum reaction energy barrier during hydrolysis. In addition, the hydroxyl groups on the surface are also able to provide an H-transfer for the generation of  $CH_4$  as well as free O atoms for the formation of S–O bonds. The depletion of surface hydroxyl groups can be replenished by the dissociation of  $H_2O$  molecules, which effectively enhances the role of  $H_2O$  molecules in the hydrolysis reaction.

The reaction processes of Routes VIII and VI are analogous. According to the alteration of reaction energy barriers,  $ZrO_2$  facilitates the entire hydrolysis process. Nevertheless,  $ZrO_2$  did not alter the rate-determining step of the hydrolysis reaction of  $C_2H_6S$ . When comparing Routes VII and VIII,  $ZrO_2$  and hydroxyl exhibited disparate different catalytic effects, and the introduction of hydroxyl was capable of further reducing the maximum reaction energy barrier.



The co-promotion of  $\text{ZrO}_2$  and hydroxyl groups was found to reduce the maximum reaction energy barriers of  $\text{CH}_3\text{SH}$  by  $173.61 \text{ kJ mol}^{-1}$  and  $145.89 \text{ kJ mol}^{-1}$ , respectively. Furthermore, hydroxyl-modified  $\text{ZrO}_2$  was observed to facilitate the hydrolysis process of  $\text{CH}_3\text{SH}$  to a greater extent than that of  $\text{C}_2\text{H}_6\text{S}$ .

### 3.4 Catalysis reaction mechanism of $\text{CH}_3\text{SH}$ and $\text{C}_2\text{H}_6\text{S}$ over hydroxyl-modified $\text{ZrO}_2$

Based on the aforementioned findings, hydroxyl-modified  $\text{ZrO}_2$  has been demonstrated to enhance and modify the hydrolysis reaction process of  $\text{CH}_3\text{SH}$  and  $\text{C}_2\text{H}_6\text{S}$ . Consequently, a reaction mechanism for the hydrolysis of  $\text{CH}_3\text{SH}$  and  $\text{C}_2\text{H}_6\text{S}$  on the hydroxyl-modified  $\text{ZrO}_2$  surface has been proposed and depicted in Fig. 8.

As illustrated in Fig. 8, the hydroxyl group on the  $\text{ZrO}_2$  surface facilitated the production of  $\text{H}_2\text{S}$  and the formation of C–O bonds by providing free H atoms and free O atoms. Furthermore, the surface-free O atoms can effectively immobilize the intermediates  $\text{CH}_3$  and  $\text{CH}_3\text{S}$ . The hydroxyl groups consumed on the surface can be replenished by the dissociation of  $\text{H}_2\text{O}$  molecules, maintaining the continuity of the hydrolysis reaction involving the hydroxyl groups. The hydrolysis of  $\text{CH}_3\text{SH}$  on the surface of hydroxyl-modified  $\text{ZrO}_2$  proceeds as follows:  $\text{CH}_3\text{SH} (+\text{H}_2\text{O}) \rightarrow \text{CH}_3\text{O} (+\text{H}_2\text{S}) \rightarrow \text{CH}_3\text{OH} (+\text{H}_2\text{S})$ . The hydrolysis process of  $\text{C}_2\text{H}_6\text{S}$  on the hydroxyl-modified  $\text{ZrO}_2$  surface proceeds as follows:  $\text{C}_2\text{H}_6\text{S} (+\text{H}_2\text{O}) \rightarrow \text{CH}_3\text{SO} (+\text{H}_2\text{O} + \text{CH}_4) \rightarrow \text{CH}_3\text{SHO} (+\text{CH}_4) \rightarrow \text{H}_2\text{S} + \text{CH}_2 (+\text{CH}_4) \rightarrow \text{HCHO} (+\text{CH}_4 + \text{H}_2\text{S})$ .

## 4. Conclusions

This work investigates the competitive adsorption process of  $\text{CH}_3\text{SH}$ ,  $\text{C}_2\text{H}_6\text{S}$ , and  $\text{H}_2\text{O}$  on the surface of hydroxyl-modified  $\text{ZrO}_2$  using a density functional theory approach. Additionally, a detailed catalytic hydrolysis reaction mechanism is proposed. The adsorption process of  $\text{CH}_3\text{SH}$ ,  $\text{C}_2\text{H}_6\text{S}$ , and  $\text{H}_2\text{O}$  on the surface of hydroxyl-modified  $\text{ZrO}_2$  is attributed to chemisorption, with the Zr–S, H–O and H–Zr bonds playing a role. There is no competitive adsorption relationship between  $\text{H}_2\text{O}$  and

$\text{CH}_3\text{SH}/\text{C}_2\text{H}_6\text{S}$ , but there is competitive adsorption between  $\text{CH}_3\text{SH}$  and  $\text{C}_2\text{H}_6\text{S}$ . It reveals the water-resistant properties of hydroxyl-modified  $\text{ZrO}_2$  in desulfurization. The adsorption of  $\text{CH}_3\text{SH}$  on the Zr top site is favored over that of  $\text{C}_2\text{H}_6\text{S}$ . The hydrolysis of  $\text{CH}_3\text{SH}$  and  $\text{C}_2\text{H}_6\text{S}$  is a heat-absorbing process that cannot occur spontaneously. The formation of  $\text{CH}_3\text{O}$  and the fracture of  $\text{CH}_3\text{SHO}$  are the rate-determining steps for  $\text{CH}_3\text{SH}$  and  $\text{C}_2\text{H}_6\text{S}$  catalytic hydrolysis, respectively. The hydroxyl groups consumed on the surface can be replenished by the dissociation of  $\text{H}_2\text{O}$  molecules. The hydroxyl group on the  $\text{ZrO}_2$  surface facilitated the production of  $\text{H}_2\text{S}$  and the formation of C–O bonds by providing free H atoms and free O atoms, enhancing the hydrolysis of  $\text{CH}_3\text{SH}$  and  $\text{C}_2\text{H}_6\text{S}$ . It provides theoretical guidance for industrial applications and the design of hydroxyl-containing hydrolysis catalysts.

## Data availability

The data supporting this article have been included as part of the ESI.†

## Author contributions

Xin Song contributed to the study's conception and design. Calculation, data collection and analysis were performed by Xin Song and Guihua Zhang. Guihua Zhang wrote the main manuscript text. All authors read and approved the final manuscript.

## Conflicts of interest

There are no conflicts to declare.

## Acknowledgements

This work was supported by the National Natural Science Foundation of China (22006058).

## Notes and references

- 1 P. J. Liang, D. C. Cheng, H. Y. Xu, C. Y. Xu, G. W. Chu, H. K. Zou, B. C. Sun and J. F. Chen, *Sep. Purif. Technol.*, 2024, **346**, 127374.
- 2 W. Jiang, Z. Li, X. Kang, L. Luo, Y. Zhou, Q. Liu, K. Liu, X. Ji and G. He, *Gas Sci. Eng.*, 2024, **123**, 205243.
- 3 G. Zhang, Q. Zhu, W. Zhang, Y. Zheng, Y. Cao, S. Liang, Y. Xiao, F. Liu and L. Jiang, *Inorg. Chem.*, 2022, **61**, 6083.
- 4 H. Zhang, X. Liu, H. Xiao, F. Shao, T. Yan, D. Cheng, L. Han and D. Zhang, *Chem. Eng. J.*, 2024, **485**, 150003.
- 5 X. Cao, T. Ai, Z. Xu, J. Lu, D. Chen, D. He, J. Liu, R. Tian, Y. Zhao and Y. Luo, *Sep. Purif. Technol.*, 2023, **307**, 122742.
- 6 Y. Zhang, K. Li, X. Sun, X. Song, F. Wang, C. Wang, P. Ning and H. He, *Appl. Surf. Sci.*, 2021, **567**, 150851.
- 7 T. Zhong, S. Tang, W. Huang, W. Liu, H. Zhao, L. Hu, S. Tian and C. He, *Appl. Catal., B*, 2024, **343**, 123476.
- 8 R. M. Mohamed and A. A. Ismail, *Ceram. Int.*, 2022, **48**, 12592.

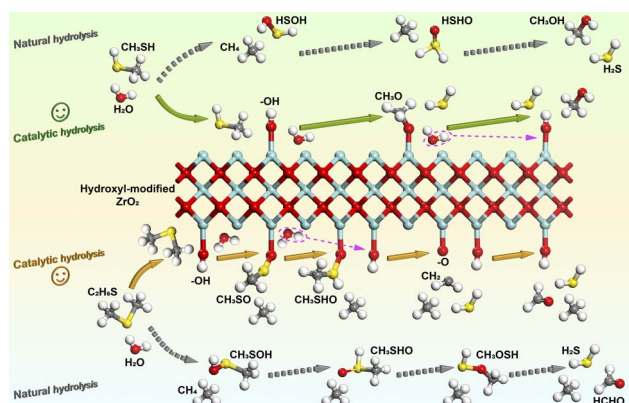


Fig. 8 Reaction mechanism of  $\text{CH}_3\text{SH}$  and  $\text{C}_2\text{H}_6\text{S}$  hydrolysis over hydroxyl-modified  $\text{ZrO}_2$ .

- 9 B. M. Alajmi, A. S. Basaleh, A. A. Ismail and R. M. Mohamed, *Surf. Interfaces*, 2023, **39**, 102899.
- 10 A. I. Ayesh and M. D. El-Muraikhi, *J. Mol. Model.*, 2022, **29**, 15.
- 11 N. Liu, P. Ning, X. Sun, C. Wang, X. Song, F. Wang and K. Li, *Sep. Purif. Technol.*, 2021, **259**, 118205.
- 12 X. Song, P. Ning, C. Wang, K. Li, L. Tang, X. Sun and H. Ruan, *Chem. Eng. J.*, 2017, **314**, 418.
- 13 X. Song, L. Sun, H. Guo, K. Li, X. Sun, C. Wang and P. Ning, *ACS Omega*, 2019, **4**, 7122.
- 14 X. Sun, W. Huang, H. Xu, Z. Qu, J. Wu and N. Yan, *Sep. Purif. Technol.*, 2023, **310**, 123194.
- 15 E. Osei-Agyemang, A. Dasan, R. Lucas, S. Foucaud, J. P. aul, S. Cristol and E. Laborde, *Appl. Surf. Sci.*, 2022, **576**, 151622.
- 16 B. Delley, *J. Chem. Phys.*, 2000, **113**, 7756.
- 17 L. Sun, P. Ning, X. Zhao, X. Song, K. Li, C. Wang, X. Sun and L. Jia, *Chem. Eng. J.*, 2021, **412**, 128752.
- 18 M. Ali, Z. Bibi, M. W. Younis and M. A. Iqbal, *Inorg. Chem. Commun.*, 2024, **160**, 111891.
- 19 J. P. Perdew, K. Burke and M. Ernzerhof, *Phys. Rev. Lett.*, 1996, **77**, 3865.
- 20 X. Song, X. Chen, L. Sun, K. Li, X. Sun, C. Wang and P. Ning, *Chem. Eng. J.*, 2020, **399**, 125764.
- 21 S. Wan, X. Song, X. Wang, C. Yuan, B. Wang, H. Chen, Y. Li, K. Ouyang and R. Chen, *Sep. Purif. Technol.*, 2022, **302**, 122158.
- 22 L. Jia, X. Song, L. Sun, S. Zhang, K. Li and P. Ning, *Chem. Eng. J.*, 2022, **429**, 132376.

